IEEE Photonics Journal
An IEEE Photonics Society Publication

Open Access

Adaptive SMF Coupling Based on Precise-Delayed SPGD Algorithm and Its Application in Free Space Optical Communication

Volume 10, Number 3, June 2018

Guan Huang
Chao Geng
Feng Li
Yan Yang
Xinyang Li

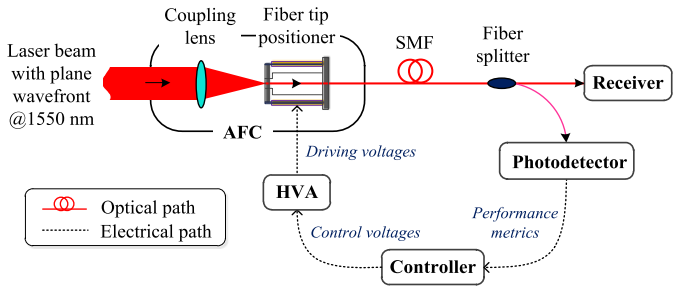

DOI: 10.1109/JPHOT.2018.2835721
1943-0655

Adaptive SMF Coupling Based on Precise-Delayed SPGD Algorithm and Its Application in Free Space Optical Communication

Guan Huang,[1,2,3] **Chao Geng**,[1,2] **Feng Li**,[1,2] **Yan Yang**,[1,2,3] **and Xinyang Li**[1,2]

[1]Key Laboratory on Adaptive Optics, Chinese Academy of Sciences, Chengdu 610209, China
[2]Institute of Optics and Electronics, Chinese Academy of Sciences, Chengdu 610209, China
[3]University of Chinese Academy of Sciences, Beijing 100049, China

DOI:10.1109/JPHOT.2018.2835721

Manuscript received March 1, 2018; revised May 6, 2018; accepted May 8, 2018. Date of publication May 29, 2018; date of current version June 7, 2018. This work was supported in part by the National Natural Science Foundation of China under Grant 61675205 and in part by the CAS "Light of West China" program. Corresponding author: Chao Geng (e-mail: blast_4006@126.com).

Abstract: The adaptive coupling of laser beam from space into single-mode fiber (SMF) plays an important role in the fiber-based free space optical communication technology. This paper investigates a kind of adaptive SMF coupling system based on a novel corrector named adaptive fiber coupler, and an improved control algorithm named precise-delayed stochastic parallel gradient descent (PD-SPGD). Compared to the SPGD algorithm used previously, PD-SPGD can compensate for the inherent response delay of the controlled system by setting a precise time delay between the disturbed voltages and the performance metrics. The experimental results show that this new algorithm increases the iteration rate from 3 to 8 kHz and decreases the convergence time from 6.3 to 2.5 ms when the static angular errors was corrected. As a result, the control bandwidth of the sinusoidal angular jitters is more than doubled. At the end, a preliminary atmospheric compensation experiment over a 520 m near-ground propagation path is conducted to verify the effectiveness of the method mentioned above.

Index Terms: Single-mode fiber coupling, adaptive fiber coupler, precise-delayed SPGD algorithm, free space optical communication.

1. Introduction

Free space optical communication (FSOC) technology has advantages of high speed, excellent privacy and large unlicensed bandwidth, and now it is considered to be a viable and attractive approach for achieving a broadband network in the future [1]–[3]. The using of common fiber optical devices such as erbium-doped fiber amplifiers (EDFAs) based on single-mode fibers (SMF) in the FSOC technology allows longer link distance, higher link capabilities and flexibility in the mechanical design [4]. In such a system, the received laser beam has to be coupled into SMF. Atmosphere turbulence, gravitational environments, machining accuracy and the vibration of receiver platform make it difficult to ensure the high and steady fiber coupling efficiency in the practical application.

The influence of the static angular errors and angular jitters caused by these disturbances has been studied extensively [5], [6].

To solve this problem, fast-steering mirror (FSM) and corresponding position sensor are often used to realize the adaptive coupling of laser beam to SMF [7], [8]. In recent years, a new adaptive-optic device named adaptive fiber coupler (AFC, also known as adaptive fiber optics collimator [9], [10]) was developed and used in adaptive SMF coupling applications [11]–[15]. Compared to FSM, AFC was designed to drive the fiber tip directly, so it has advantages of precise control, small inertia, high resonance frequency and ability for array extension. In addition, stochastic parallel gradient descent (SPGD) algorithm is usually used to calculate the appropriate control voltages for AFC to realize the accurate adaptive control of the fiber tip. The aforementioned AFC and the SPGD-based control strategy have been successfully applied in various fields, and the iteration rate of SPGD algorithm mentioned is about 625 Hz to 3 kHz [13]–[17]. However, in the field of adaptive SMF coupling, our experience shows that calibration of a static angular error requires 20 iterations for an independent AFC [13]. So, the convergence time can be calculated to more than 6.7 ms, which is barely compatible with the high correction bandwidth required for adaptive coupling in atmospheric environment, for the characteristic frequency of the turbulence-induced tip/tilt aberrations is close to 100 Hz [18].

As a typical blind optimization algorithm, the higher control bandwidth of SPGD depends on the shorter convergence time, which is determined jointly by the iteration rate and the convergence performance (i.e., the iteration number required to converge). However, in the high-speed iteration process of SPGD, the correlation between the output disturbed voltages and the input performance metrics is often affected by the response characteristics of the controlled system. A common phenomenon is that there exists a certain time delay between the captured metrics and its corresponding disturbed voltages. As the iteration rate increases, this time delay will make the convergence performance worse and even cause the divergence. In order to solve this contradiction, delayed-SPGD (D-SPGD) algorithm was proposed and successfully used to compensate for the total time delay caused by the optical wave propagation in the phase locking control of the coherent beam combining (CBC) experiments [16], [17], which makes the convergence time almost 18 times shorter [16]. Different from the above case, the optical wave propagation delay is negligible in the control loop of the AFC-based adaptive coupling system (hereafter referred to as AFC system). However, we find that this system's inherent response delay also produces the same constraint effect. Therefore, it can be expected that designing a time delay compensation algorithm which specialized for the AFC system is also important.

In this paper, we briefly presented the control structure of the AFC system, and then experimentally demonstrated an improved control algorithm named precise-delayed SPGD (PD-SPGD). In this algorithm, the sampling rate of the performance metrics is set to many times of the iteration rate, and these metrics captured during the several historical iterations are recorded in the controller memory. Therefore, compared to SPGD and D-SPGD algorithm, PD-SPGD can get more precise compensation of the time delay through specific selection of the performance metrics in the controller memory. From the following analysis, it can be seen that accurate time delay compensation is critical when dealing with the inherent response delay of the AFC system. The comparison of the experimental results proves that this algorithm can decreases the convergence time from 6.3 ms to 2.5 ms, and as a result, the AFC system has a stronger inhibitory effect on the sinusoidal angular jitters. At the end, a practical atmospheric turbulence compensation experiment with a 137-element adaptive optics (AO) system is conducted to verify the effectiveness of the AFC system based on PD-SPGD.

2. Current Situation and Problems

Fig. 1 shows the structural scheme of AFC system. The laser beam with plane wavefront is focused and coupled into a controlled tip of SMF by AFC, part of the coupled optical power is sent to the communication receiver and another is converted to voltage by a photodetector. This voltage is transferred to the controller and used as performance metrics. Two dimension control voltages

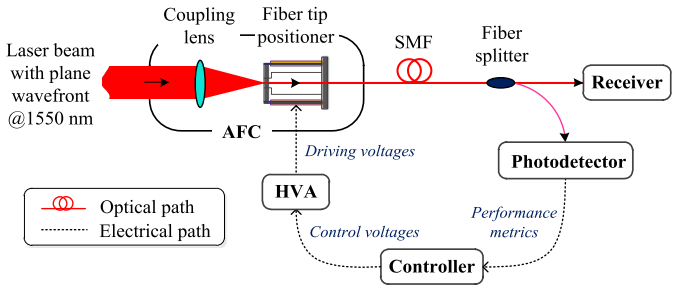

Fig. 1. Structural scheme of adaptive coupling system based on AFC.

from the controller are amplified one hundred times by the high-voltage amplifier (HVA) and then drive the AFC to realize closed loop control. Driving voltages output by the HVA are in the interval $-500\,\mathrm{V}\ldots+500\,\mathrm{V}$, and the X/Y displacements of the fiber tip are approximately in range of $\pm 30\ \mu$m, which corresponds to the tip/tilt correction range of about ± 2 mrad. The wavelength of the laser beam is $\lambda = 1550\,$nm, the effective lens aperture (beam diameter) is $D = 3.3\,$mm, the focal length of the lens is $f = 15\,$mm, and the mode field radius of the SMF is $w_0 = 5\,\mu$ m.

The controller with two channels (vertical and horizontal directions) consists of a FPGA chip and analog input/output cards. The two dimension control voltages $\mathbf{U}^{(n)} = \{u_x^{(n)}, u_y^{(n)}\}$ are updated by the conventional SPGD algorithm [21].

$$\mathbf{U}^{(n+1)} = \mathbf{U}^{(n)} + \gamma \Delta \mathbf{U}^{(n)} \left[J_+^{(n)} - J_-^{(n)} \right]. \tag{1}$$

Where n is the iteration number, γ is the step-size parameter and $\Delta\mathbf{U}^{(n)} = \{\delta u_x^{(n)}, \delta u_y^{(n)}\}$ is the random voltage perturbations. Before the algorithm performs an update, the positive disturbed voltages $\mathbf{U}^{(n)} + \Delta\mathbf{U}^{(n)}$ and negative disturbed voltages $\mathbf{U}^{(n)} - \Delta\mathbf{U}^{(n)}$ are applied to AFC in turn, and the captured performance metrics are recorded as $J_+^{(n)}$ and $J_-^{(n)}$ respectively. Period of an iteration cycle τ_{spgd} between sequential control voltage updates can be simply given by:

$$\tau_{spgd} = 2(\tau_{calc} + \tau_{resp}) \tag{2}$$

Where τ_{calc} is the time required for controller to convert metrics and perturb the voltages, τ_{resp} is the time delay between the control voltages change and the corresponding performance metrics response. The controller we used here can support the highest output update rate of about 500 kHz ($\tau_{calc} \approx 2\,\mu$ s), thus the iteration interval τ_{spgd} (usually greater than 0.3 ms in our previous experiments) in (2) may be limited to a certain extent by τ_{resp}, which refers to the sum of all the time response of HVA, AFC and photodetector in the control loop. In reality, almost all practical controlled systems are affected by response delay between the input and the output. A speculation worth thinking about in the controlled system based on SPGD is that the correlation between the captured metrics and the disturbed voltages may become weak gradually when we constantly reduce the iteration interval. For example, when the positive disturbed voltages $\mathbf{U^{(n)}} + \Delta\mathbf{U^{(n)}}$ are applied to AFC, the controller will wait for half an iteration cycle $\tau_{spgd}/2$, and then regarded the captured performance metric as $J_+^{(n)}$. However, when the τ_{resp} is considered and the iteration cycle decreases to a certain extent, the metric $J_+^{(n)}$ is not only affected by the positive disturbed voltages $\mathbf{U^{(n)}} + \Delta\mathbf{U^{(n)}}$, but also interfered by the voltages that was applied in the previous iteration. This aliasing effect will cause the fuzzy gradient estimation result of SPGD when we use (1) to update the voltages, thereby possibly affecting the convergence performance.

In order to measure τ_{resp}, we use controller to generate a series of sinusoidal waveforms with different frequencies, these signals are then amplified by HVA and drive a certain direction of AFC. The corresponding system's response, which refers to the metrics converted by photodetector, is recorded to compare with the input. The amplitude of these sine waves is about 0.05 V (which will be amplified by 100 times before being applied on the AFC), and the induced position deviation of the

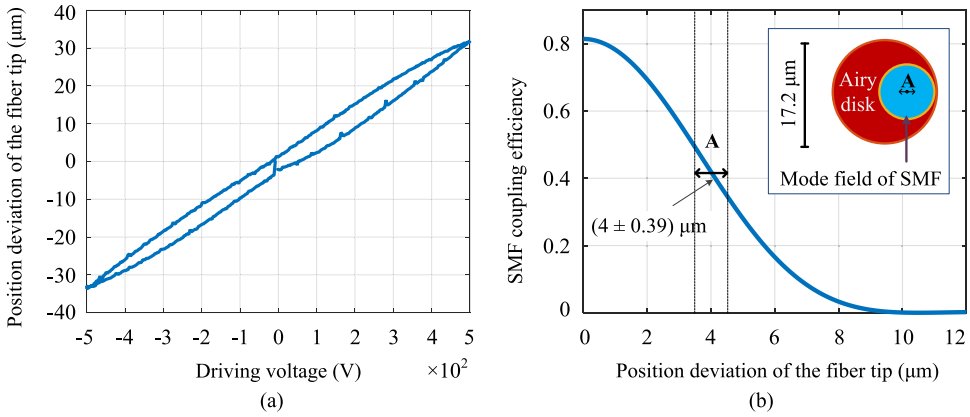

Fig. 2. (a) Position deviation of the fiber tip as the function of AFC's driving voltage; (b) SMF coupling efficiency as the function of position deviation of the fiber tip and the corresponding sketch of the initial position of the fiber tip.

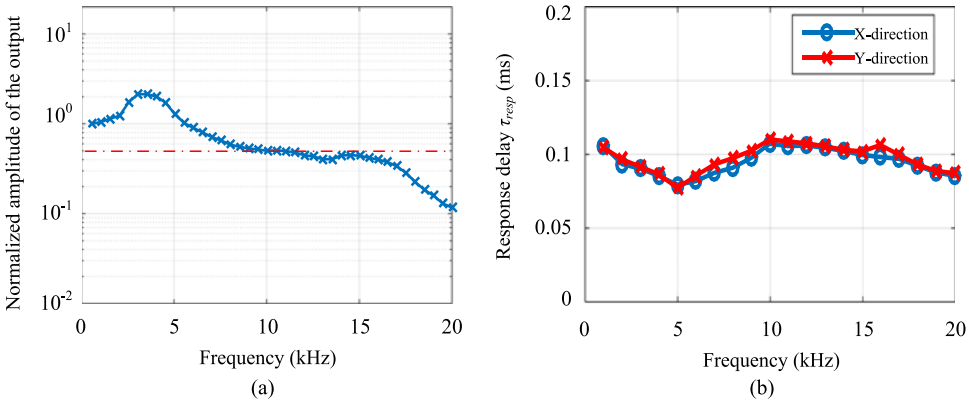

Fig. 3. (a) Normalized dithering amplitude of the performance metrics as the function of the frequency; (b) Calculation of τ_{resp} within 10 kHz.

fiber tip is about ± 0.39 μm in the low frequency range, which is close to the perturbation amplitude (usually ranged from 0.1 μm to 0.5 μm) of the SPGD algorithm in our previous experiments.

Fig. 2(a) shows the relationship between the AFC's driving voltages and the induced position deviation of the fiber tip, and we can find that there is an approximate linear relationship between them. Fig. 2(b) shows the relationship between the SMF coupling efficiency (which is proportional to the performance metrics provided by photodetector) and the position deviation of the fiber tip through simulation [6]. According to Fig. 2(b), we set the initial position of the fiber tip to be 4 μm from the center of the focal spot, to make the system's response similar to the linear correlation with the test sine signals. Response delay τ_{resp} can be calculated by the relative phase delay between the input and the output. For example, if phase delay is about π (a half period) when the frequency of input is 5 kHz, τ_{resp} is about 0.1 ms (0.5/5000).

Fig. 3(a) shows the relationship between the normalized dithering amplitude of the performance metrics (the average of both two directions) and the frequency of the test sine signals. It can be seen that when the test frequency is beyond 10 kHz, the dithering amplitude of the performance metrics drops to be less than half of the original, which might cause that the corresponding phase delay between the input and the output cannot be calculated accurately. Therefore, we only calculated the inherent response delay when the frequency is within 10 kHz, as shown in Fig. 3(b). We can find that the τ_{resp} is a nearly constant when the frequency of test sine signal is within 10 kHz. The

response delay of *X*-direction is ranged from 79 μs to 107 μs and *Y*-direction is ranged from 77 μs to 110 μs, and their average value is 95 μs and 97 μs respectively. That is, when the voltages are applied to a certain direction of AFC, performance metrics will respond after about 0.1 ms due to the response delay τ_{resp}. Consequently, a threshold of the iteration rate is about 5 kHz ($\tau_{spgd} = 0.2$ ms). It means that when the iteration rate is too close to 5 kHz, the correlation between the captured metrics and the disturbed voltages starts to weaken, and the convergence performance of SPGD starts to deteriorate. In extreme cases, when the iteration rate exceeds 5 kHz, the captured metrics will be completely irrelevant to the disturbed voltages, and the SPGD algorithm starts to diverge. Due to the shorter convergence time is determined jointly by the iteration rate and the convergence performance, a reasonable iteration rate is about 3 kHz in our actual test, to reach a compromise on the deterioration of corresponding convergence performance.

3. Precise-Delayed SPGD Algorithm

Therefore, we need to readjust the correlation between the captured metrics and the disturbed voltages by compensating τ_{resp}. Since it is an approximate constant value, one way that might work is to set a controllable time delay. This idea is originated from D-SPGD algorithm, which was proposed by Weyrauch *et al*. and had been successfully used in CBC experiments [16], [17]. Different from the above case, the iteration rate of 500 kHz (which is determined by τ_{calc}) cannot be achieved by simply compensating τ_{resp} in the AFC system. Because the attenuated variation of performance metrics (which is mainly decided by the amplitude-frequency characteristics of AFC system) and the limited conversion accuracy of analog to digital converter (ADC) used here cannot be neglected when the frequency of the control voltages is gradually increased. As shown in Fig. 3(a), when the frequency of the test sine signal increases to 20 kHz, the dithering amplitude of the performance metrics has dropped to roughly one-tenth of its original value. In the high-speed iteration process, this phenomenon and τ_{resp} together determine the convergence performance of SPGD. In our actual test, the inherent response delay τ_{resp} has a dominant influence on the convergence performance when the iteration rate is within 8 kHz. Therefore, the corresponding iteration interval τ_{spgd} (within 0.125 ms) can be obtained after compensation is not different than τ_{resp} (about 0.1 ms in two directions), this precludes utilization of D-SPGD algorithm in the AFC system's inherent response delay compensation, for its minimum compensation unit is a complete iteration cycle, which can easily result in the inadequate compensation or overcompensation. We need to set a controllable time delay in a more careful and precise manner.

In the proposed PD-SPGD algorithm, the sampling rate of the performance metrics is set to many times of the iteration rate, and these metrics captured during the several historical iterations are recorded in the controller memory. Here, we use parameter *K* to represent the ratio between the sampling rate and iteration rate, i.e., the number of metrics recorded within one iteration interval. Parameter *M* is used to represent the number of historical iterations in which the metrics are recorded. At each iteration (*n*), we can take a specific selection from these metrics (represented here as $J_0^{(n)}, J_1^{(n)}, \ldots, J_{MK}^{(n)}$) in the controller memory to perform the gradient estimation, and update the control voltages from $\mathbf{U}^{(n)}$ to $\mathbf{U}^{(n+1)}$. Here, to expect that the selected metrics are located at the center of the delayed metrics, we added a parameter τ_{comp} to represent the designed compensation time of PD-SPGD. It can be determined by the following formula:

$$\tau_{comp} = \tau_{resp} + \tau_{spgd}/4. \tag{3}$$

From the description above, the control voltages $\mathbf{U^{(n)}} = \{u_x^{(n)}, u_y^{(n)}\}$ are updated by the modified rule:

$$\mathbf{U}^{(n+1)} = \mathbf{U}^{(n)} + \gamma \Delta \mathbf{U}^{(n-\Delta n)} \left[J_p^{(n)} - J_{p+K/2}^{(n)} \right] \tag{4}$$

Here, $\Delta \mathbf{U}^{(n-\Delta n)}$ is the random perturbations disturbed in the iteration (n-Δn). $J_p^{(n)}$ and $J_{p+k/2}^{(n)}$ are the selected metrics that corresponding to the disturbed voltages $\mathbf{U}^{(n-\Delta n)} + \Delta \mathbf{U}^{(n-\Delta n)}$ and $\mathbf{U}^{(n-\Delta n)} - \Delta \mathbf{U}^{(n-\Delta n)}$. The integer number Δn and p are defined as the integral-delay parameter and the

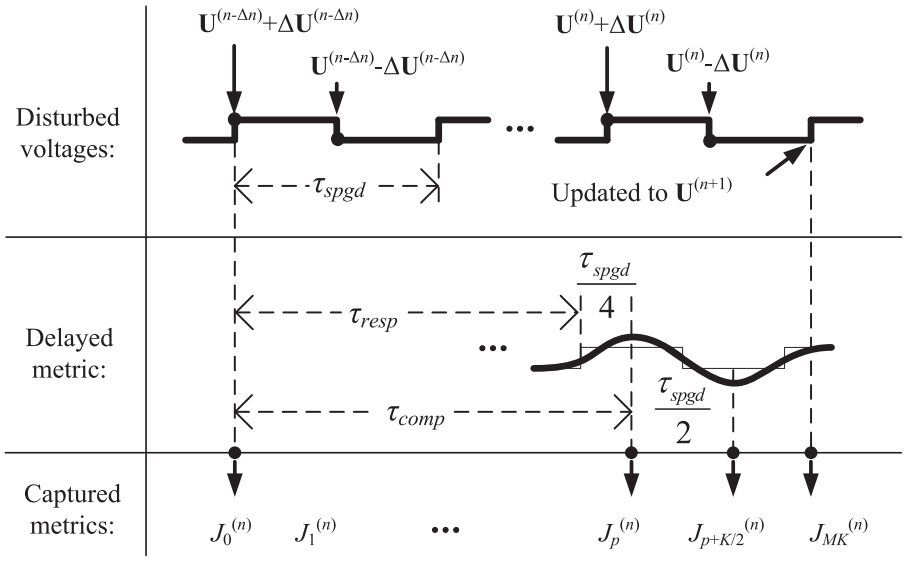

Fig. 4. The implementation flowchart of PD-SPGD algorithm.

TABLE 1
Three kinds of Algorithms under Different Parameter Settings

Parameter / Algorithm	Integral-delay parameter Δn	Precise-delay parateyer p
SPGD	0	$K/2$
D-SPGD	int $<\tau_{resp}/\tau_{spgd}>$	MK-$K/2$
PD-SPGD	int $<\tau_{comp}/\tau_{spgd}>$	int$<K\tau_{comp}/\tau_{spgd}>$

precise-delay parameter respectively, which can be calculated by the following formula:

$$\Delta n = \text{int} < \tau_{comp}/\tau_{spgd} >,\ p = \text{int} < K\,\tau_{comp}/\tau_{spgd} > \tag{5}$$

The operator "int $< >$" used here denotes integer conversion. Note that the computing method of parameter Δn is similar to the D-SPGD. The newly added parameter p represents the location of selected metrics $J_p^{(n)}$ and $J_{p+K/2}^{(n)}$ in the set of $\{J_0^{(n)}, J_1^{(n)}, \ldots, J_{MK}^{(n)}\}$. Parameter K determines the accuracy of the compensation that can be achieved, it is usually set to an integer bigger than 10. Parameter M is usually set to $\Delta n + 1$, to ensure that all these metrics are sampled during the period between the disturbed voltages change and the corresponding metrics response.

In reality, due to the limited compensation accuracy, we use τ'_{comp} to describe the actual compensation time of PD-SPGD. It can be determined by the following formula:

$$\tau'_{comp} = \frac{p}{K} \times \tau_{spgd} \tag{6}$$

Fig. 4 shows the implementation flowchart of PD-SPGD algorithm without considering the compensation accuracy, that is, $\tau'_{comp} = \tau_{comp}$.

Note that the SPGD and D-SPGD algorithm are particular cases of PD-SPGD algorithm under different parameter settings, as shown in the Table 1.

One interesting thing is that, taking (6) into Table 1 and use $M = \Delta n + 1$ for parameter replacements, we can calculate that the τ'_{comp} of SPGD and D-SPGD algorithm is $0.5\tau_{spgd}$ and

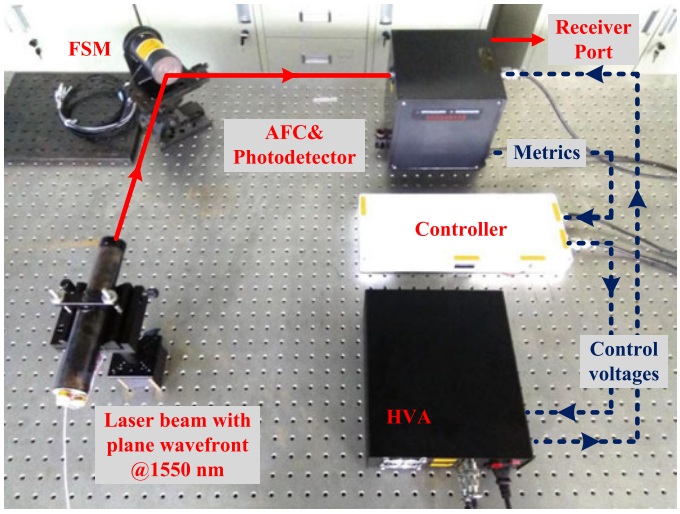

Fig. 5. Experimental setup diagram of the AFC system.

$(0.5+\Delta n)\tau_{spgd}$ respectively. This result is reasonable; because for the SPGD algorithm, when the disturbed voltages $\mathbf{U}^{(n)}+\Delta\mathbf{U}^{(n)}$ and $\mathbf{U}^{(n)}-\Delta\mathbf{U}^{(n)}$ are applied to AFC, the corresponding metrics $J_+^{(n)}$ and $J_-^{(n)}$ will be captured after half a cycle, and these two halves make up an entire iteration interval. The effect of D-SPGD algorithm is to set an integer periodic delay on the basis of the semi-periodic delay of SPGD.

4. Comparison Experiments With Angular Errors

Experiments of SMF coupling under static angular error of 367 μrad and sine angular jitter with amplitude of 166 μrad (which is equal to 5.5 μm and $\pm$2.5 μm misalignment errors at the fiber tip) are demonstrated respectively. These errors are introduced using a FSM, which placed in front of the AFC. Fig. 5 shows the experimental setup diagram.

The iteration rate of PD-SPGD algorithm set up here is 8 kHz and the sampling rate is 80 kHz, thus $\tau_{spgd}=125\,\mu$ s, $K=10$, and the compensation accuracy is 12.5 μs. To compensate for 96 μs response delay (the average value of the two directions), we can figure that $\tau_{comp}\approx 127\,\mu$s, $\Delta n=1$, $p=10$ (the closest integer number to 127/125 and 1270/125), and the actual compensation time of PD-SPGD is $\tau'_{comp}=125\,\mu$s. Another key parameter M is equal to 2 in this case, so the corresponding recorded metrics can be expressed as $J_0^{(n)}, J_1^{(n)}, \ldots, J_{20}^{(n)}$ at each iteration (n), and the selected metrics of PD-SPGD are $J_{10}^{(n)}$ and $J_{15}^{(n)}$. In order to verify the effectiveness of this proposed algorithm, a series of experiments under different parameters settings are conducted. Convergence time t_{conv} is used to evaluate the corrective performance, which is equal to the time needed for the normalized performance metrics J rise to 90%.

As shown in Fig. 6, when the delay parameters $\Delta n=0$ and $p=5$, which is equivalent to using SPGD algorithm with τ'_{comp} of 65.2 μs, the iteration curve diverges. When parameters $\Delta n=1$ and $p=8$,10,12, which is equivalent to using PD-SPGD algorithm with τ'_{comp} of 100 μs, 125 μs, and 150 μs respectively, the iteration curve starts to converge and the convergence time t_{conv} can be counted as 55 ms, 2.5 ms, and 137.5 ms respectively by 20 sets of data. Finally, when parameters $\Delta n=1$ and $p=15$, which is equivalent to using D-SPGD algorithm with τ'_{comp} of 187.5 μs, the iteration cure starts to diverge again. In this experiment, it can be seen that the shortest convergence time will be obtained only when the PD-SPGD algorithm (with appropriate parameter setting) is used. Fig. 7(a) shows the detailed view of iteration curve when $\Delta n=1$ and $p=10$, where we can find that the correcting process only takes about 20 iterations. In our best

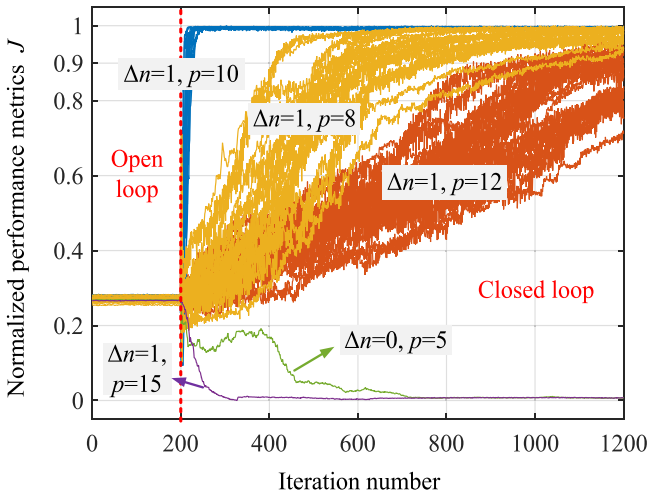

Fig. 6. Iteration curve of different delay parameters settings in the static angular errors correction experiment.

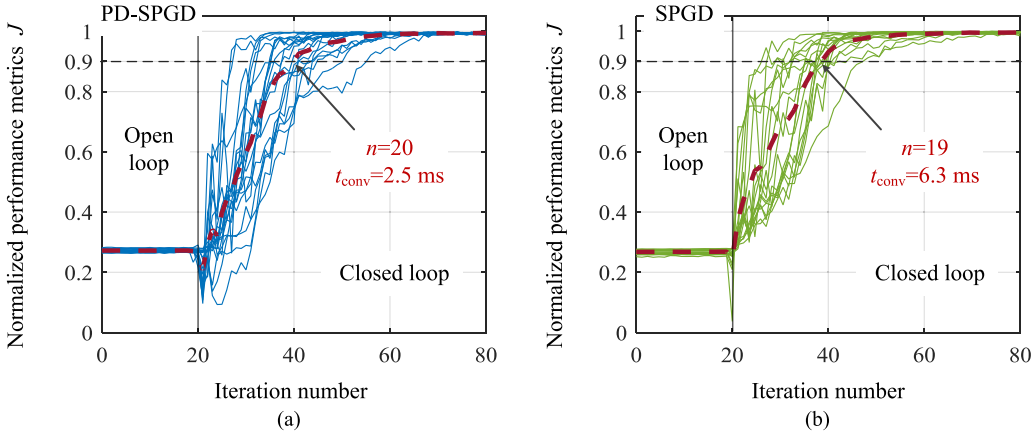

Fig. 7. (a) Iteration curve of PD–SPGD with compensation time of 125 μs and iteration rate of 8 kHz. (b) Iteration curve of SPGD with iteration rate of 3 kHz.

previous experiment, this value is 19 with the SPGD algorithm at a lower iteration rate of 3 kHz, and the convergence time t_{conv} is 6.3 ms, as shown in Fig. 7(b). This results tell that PD-SPGD algorithm can improve the iteration rate without increasing the iteration number needed to converge, and thus the actual convergence time is 2.5 times shorter than before (6.3/2.5 $\approx$ 2.5).

Sine angular jitter with frequency of 100 Hz and amplitude of 166 μ rad is loaded on the plane wave, and the experimental results of adaptive coupling using SPGD and PD-SPGD are shown in Fig. 8, where the iteration rate is 3 kHz and 8 kHz respectively and each algorithm works on their optimal state. From iterations 1 to 2000, the metrics J are sinusoidally varying with an average value of 0.81, and mean square error (MSE) of 0.13; from iterations 2001 to 4000, the SPGD algorithm is used, and the average of J decreased to 0.79 with MSE of 0.14; from iterations 4001 to 6000, the PD-SPGD algorithm is employed, and the average of J increases to 0.97 with MSE of 0.019. Therefore, compared to the SPGD algorithm, PD-SPGD with higher iteration rate can significantly improve the dynamic performance of AFC system. It makes the average of J up by 19.8% and MSE down by 86.4%, whereas the SPGD algorithm apparently accomplishes the opposite effect.

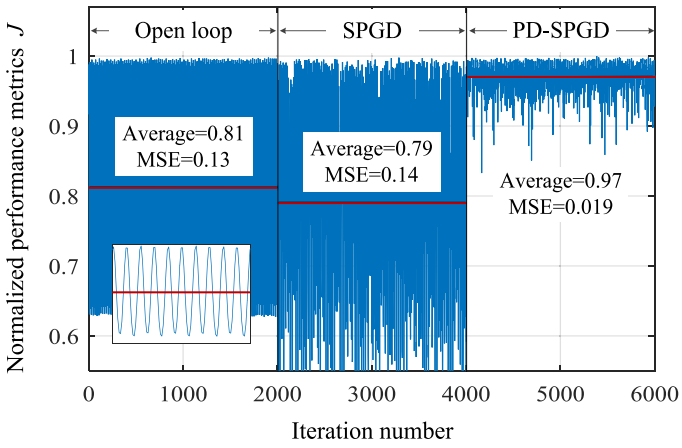

Fig. 8. Comparison between SPGD and PD-SPGD algorithm at sine angular jitter of 100 Hz.

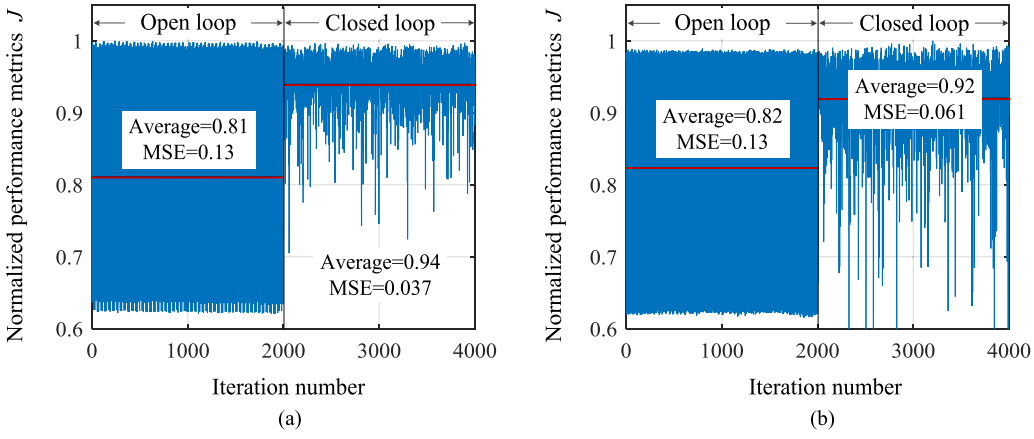

Fig. 9. (a) PD-SPGD algorithm calibration experiment at the frequency of sine jitters is 150 Hz and (b) 200 Hz respectively.

Correction performance of PD-SPGD is shown in Fig. 9, where the frequency of angular jitters is modified to be 150 Hz and 200 Hz. The average of J went up by 16% in Fig. 9(a) and 12.2% in Fig. 9(b), and MSE went down by 71.5% and 53.1% respectively. It can be seen that the average of J in closed loop has not changed much when the input disturbance's frequency increased from 150 Hz to 200 Hz, yet the corresponding MSE almost doubled. As a result, the minimum value of J begins to be less than that in open loop, which will have a negative impact on the bit error rate of the communication terminal. Therefore, we think that PD-SPGD algorithm reaches its calibration limit when the frequency of angular jitters is 200 Hz. However, it is clearly that the corrective performance of PD-SPGD is still better than SPGD algorithm under sine angular jitters of 100 Hz. This result confirms that the decrease of the convergence time can improve the control bandwidth of angular jitters by more than two times.

5. Experiments Under Actual Atmospheric Turbulence

In the remainder of this paper, an example resulting from the preliminary experiments for actual atmospheric turbulence correction using AFC system is presented. The experiment described here was also performed with an AO system [19], [20], which had a 0 dB error suppression bandwidth of about 50 Hz and was placed at the front of the AFC system. Beacon light with a wavelength of

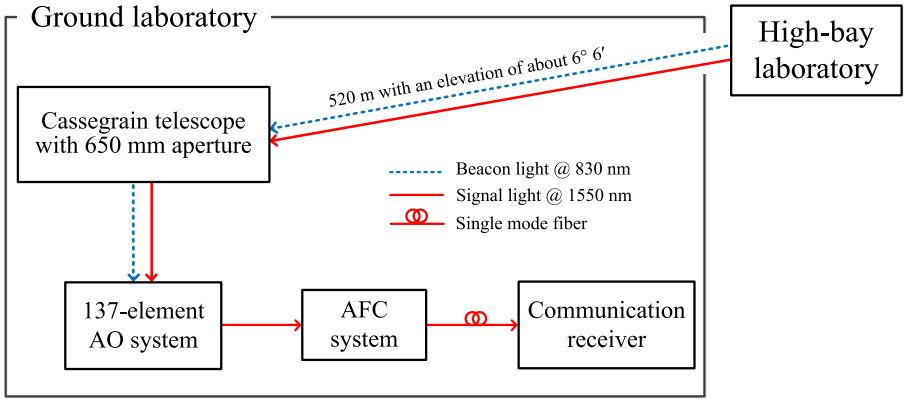

Fig. 10. Schematic of the experimental setup and the optical path used in the actual atmospheric compensation experiments.

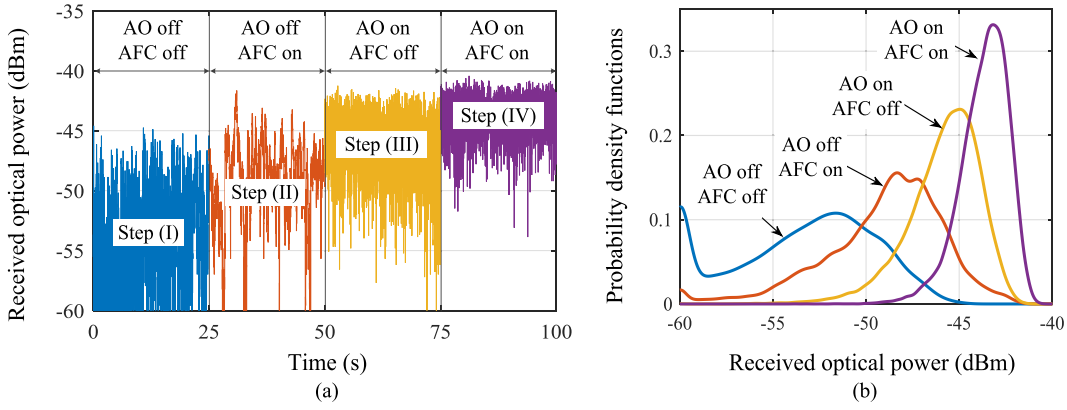

Fig. 11. (a) Sample evolution curve of received optical power in dependence on the time. (b) Probability density functions (PDFs) calculated from measured optical power values for the four different operation conditions.

830 nm was used for AO and signal light with a wavelength of 1550 nm was used for beam coupling and communication. These two kinds of light were received by a Cassegrain telescope with an aperture of 650 mm. The AO system contains a 137-element deformable mirror, a FSM, a Hartmann-Shack wavefront sensor, and a wavefront controller. The structural parameters of the AFC system were the same as above and the PD-SPGD algorithm with iteration rate of 8 kHz was used. The split ratio of the fiber splitter for photodetector and communication receiver was 5: 95. These two systems and the telescope were located at a ground laboratory on one side, the beacon light and signal light emission equipment was located at the high-bay laboratory building on the other side. The distance was about 520 m with an elevation of about 6°6′. The schematic of the experimental setup and the optical path is shown in Fig. 10. One experimental result performed under relatively strong turbulence conditions (Fried parameter r_0 is 2.6 cm) are shown in Fig. 11. The operation status of the two systems contains four different steps: (I) two systems didn't perform any correction; (II) only the AFC correction was performed; (III) only AO correction was performed; (IV) both AFC and AO performed corrections.

Fig. 11(a) shows a sample evolution curve for the received optical power, which is measured at the receiver port of AFC system. By means of only correcting static angular errors and angular jitters with AFC system in step (II), the average of optical power is increased from −51.53 dBm to −47.57 dBm; when the higher-order aberrations is corrected by AO system in step (III), this value becomes −44.98 dBm; finally, when two systems work simultaneously in step (IV), the average

of received optical power reaches the optimal value, that is −43.00 dBm. It can be calculated that compared to the previous step, the average value of optical power went up by 3.95 dB in step (II) and went up by 1.98 dB in step (IV). The dithering range of optical power in step (I) is 15.86 dB; this index is slightly worse in step (II) and step (III), which are 18.81 dB and 19.21 dB; the dithering range is suppressed to the optimal value when both systems are closed in step (IV), which is 13.44 dB. Fig. 11(b) presents the probability density functions (PDFs) of the received optical power, calculated for each of the four different operation conditions. The PDF in step (I) is wide and bumpy, which indicates that the coupling efficiency is unstable and degraded by the atmospheric turbulence; these curves gradually become narrower and shift to larger optical power direction in subsequent steps, which indicates that the stable and promoted coupling efficiency is achieved.

The above experimental results tell that the AFC system can effectively improve the average value of received optical power and suppress the power fluctuation in both cases of AO system off and on. In addition, the corrective performance in step (II) is worse than that in step (III). Due to the optical power coupled into the SMF is used as the feedback signal by AFC system, its performance cannot be fully realized when this power is too low to be detected. As in step (II), note that −60 dBm is equivalent to 1 nW at the receiver port and 53 pW at the photodetector port, whereas the photosensitivity of the photodetector used in this experiment is 1.7×10^8 V/W, so the corresponding voltage signal is only 9 mV, which is close to the noise level for the ADC of controller. The advantage of this control structure is that it can correct the misalignment errors caused by the movement of the receiving platform, and it also has a stronger inhibitory effect on the dithering of focused spot which comes from the tip/tilt residual errors of AO system. As a result, the AFC system can continue to improve the coupling performance in step (IV). Comprehensive and detailed analyses of the AFC systems' atmospheric compensation capabilities are subject of ongoing studies and will be presented in future papers.

6. Conclusion

We have demonstrated an AFC-based adaptive SMF coupling system and an improved control algorithm named PD-SPGD. This system could be used for corrections of static angular errors and angular jitters to realize the stable and efficient coupling of space laser into SMF, which is crucial for the fiber-based FSOC technology. It is shown that the AFC system's inherent response delay τ_{resp} (close to 0.1 ms in both directions) limits the convergence performance of SPGD algorithm in the high-speed iteration process. When the compensation is implemented by PD-SPGD algorithm, the iteration rate increases from 3 kHz to 8 kHz and the statistic value of the iteration number required for convergence is much the same as before, so the convergence time decreases from 6.3 ms to 2.5 ms. As a result, the actual control bandwidth of the angular jitters improves by almost the same proportion. In the end, a preliminary adaptive SMF coupling experiment with the AFC system and the 137-element AO system was carried out in the real atmospheric turbulence with a 520 m horizontal distance. Experimental results tell that the AFC system can further improve the coupling efficiency in both cases of the AO system off and on; however, the calibration of AFC system cannot be fully realized where the presence of higher-order aberrations make it difficult to detect the performance metrics. In addition, technical research of AFC array combined with the mentioned new algorithm is an ongoing effort in our group [14], [15], which is expected to solve the above problems in the future.

References

[1] K. P. Peppas and P. T. Mathiopoulos, "Free-space optical communication with spatial modulation and coherent detection over HK atmospheric turbulence channels," *J. Lightw. Technol.*, vol. 33, no. 20, pp. 4221–4232, Oct. 2015. Art. no. 7902410.

[2] Y. Wang, D. Wang, and J. Ma, "On the performance of coherent OFDM systems in free-space optical communications," *IEEE Photon. J.*, vol. 7, no. 4, Aug. 2015, Art. no. 7902410.

[3] G. Milione *et al.*, "4 × 20 Gbits/s mode division multiplexing over free space using vector modes and q-plate mode (de)multiplexer," *Opt. Lett.*, vol. 40, no. 9, pp. 1980–1983, Apr. 2015.
[4] D. V. Hahn, D. M. Brown, N. W. Rolander, J. E. Sluz, and R. Venkat, "Fiber optic bundle array wide field-of-view optical receiver for free space optical communications," *Opt. Lett.*, vol. 35, no .21, pp. 3559–3561, Oct. 2010.
[5] M. Toyoshima, "Maximum fiber coupling efficiency and optimum beam size in the presence of random angular jitters for free-space laser systems and their applications," *J. Opt. Soc. Amer. A*, vol. 23, no. 9, pp. 2246–2250, Apr. 2006.
[6] J. Ma, F. Zhao, L. Tan, S. Yu, and Q. Han, "Plane wave coupling into single-mode fiber in the presence of random angular jitters," *Appl. Opt.*, vol. 48, no. 27, pp. 5184–5189, Sep. 2009.
[7] R. Zhang, J. Wang, G. Zhao, and J. Lv, "Fiber-based free-space optical coherent receiver with vibration compensation mechanism," *Opt. Exp.*, vol. 21, no. 15, pp. 18434–18441, Jul. 2013.
[8] H. Takenaka, M. Toyoshima, and Y. Takayama, "Experimental verification of fiber-coupling efficiency for satellite-to-ground atmospheric laser downlinks," *Opt. Exp.*, vol. 20, no. 14, pp. 15301–15308, Jul. 2012.
[9] M. Vorontsov, T. Weyrauch, L. Beresnev, G. Carhart, L. Liu, and K. Aschenbach, "Adaptive array of phase-locked fiber collimators: analysis and experimental demonstration," *IEEE J. Sel. Topics Quantum Electron.*, vol. 15, no. 2, pp. 269–280, Jan. 2009.
[10] C. Geng, X. Li, X. Zhang, and C. Rao, "Coherent beam combination of an optical array using adaptive fiber optics collimators," *Opt. Commun.* vol. 284, no. 24, pp. 5531–5536, Dec. 2011.
[11] C. Geng *et al.*, "A kind of control system of adaptive fiber coupler/collimator for laser beam transceiving propagation," Chinese Patent, Patent Number: ZL201310161222.7, 2016.
[12] C. Geng, G. Huang, X. Li, F. Li, and Y. Yang, "A kind of single-mode fiber adaptive coupling system based on two-dimensional scanning of the fiber tip," Chinese Patent Application, Patent Pending Number: 201710145247.6, 2017.
[13] W. Luo, C. Geng, Y. Wu, Y. Tan, H. Liu, and X. Li, "Experimental demonstration of single-mode fiber coupling using adaptive fiber coupler," *Chin. Phys. B*, vol. 23, no. 1, pp. 014207-1–014207-6, 2014.
[14] F. Li, C. Geng, X. Li, and Q. Qiu, "Co-aperture transceiving of two combined beams based on adaptive fiber coupling control," *IEEE Photon. Technol. Lett.*, vol. 27, no. 17, pp. 1797–1790, Jun. 2015.
[15] F. Li, C. Geng, G. Huang, Y. Yang, X. Li, and Q. Qiu, "Experimental demonstration of coherent combining with tip/tilt control based on adaptive space-to-fiber laser beam coupling," *IEEE Photon. J.*, vol. 9, no. 2, Apr. 2017, Art. No. 7102812.
[16] T. Weyrauch *et al.*, "Experimental demonstration of coherent beam combining over a 7 km propagation path," *Opt. Lett.*, vol. 36, no. 22, pp. 4455–4457, Nov. 2011.
[17] T. Weyrauch *et al.*, "Deep turbulence effects mitigation with coherent combining of 21 laser beams over 7 km," *Opt. Lett.*, vol. 41, no. 4, pp. 840–843, Feb. 2016.
[18] J. W. Hardy, *Adaptive Optics for Astronomical Telescope*. New York, NY, USA: Oxford Univ. Press, 1998.
[19] M. Chen, C. Liu, and H. Xian, "Experimental demonstration of single-mode fiber coupling over relatively strong turbulence with adaptive optics," *Appl. Opt.*, vol. 54, no. 29, pp. 8722–8726, Oct. 2015.
[20] M. Chen, C. Liu, and H. Xian, "Experimental results of 5-Gbps free-space coherent optical communications with adaptive optics," *Opt. Commun.*, vol. 418, pp. 115–119, Mar. 2018.
[21] M. Vorontsov, G. Carhart, and J. Ricklin, "Adaptive phase-distortion correction based on parallel gradient-descent optimization," *Opt. Lett.*, vol. 22, no. 12, pp. 907–909, Jun. 1997.